1 **Photoenhanced sulfates formation by the heterogeneous uptake of SO_2 on non-**

2 **photoactive mineral dust**

3 Wangjin Yang, Jiawei Ma, Hongxing Yang, Fu Li, Chong Han*

4 School of Metallurgy, Northeastern University, Shenyang, 110819, China

5 *Address correspondence to author: hanch@smm.neu.edu.cn

7 **Short summary.** We provide evidence that light prominently enhances the conversion of SO_2

8 to sulfates on non-photoactive mineral dust, where triplet states of SO_2 ($^3SO_2$) can act as a

9 pivotal trigger to generate sulfates. Photochemical sulfate formation depends on H_2O, O_2, and

10 basicity of mineral dust. The SO_2 photochemistry on non-photoactive mineral dust significantly

11 contributes to sulfates, highlighting previously unknown pathways to better explain the missing

12 sources of atmospheric sulfates.

14 **Abstract.** Heterogeneous uptake of SO_2 on mineral dust is a predominant formation pathway

15 of sulfates, whereas the contribution of photo-induced SO_2 oxidation to sulfates on the dust

16 interfaces still remains unclear. Here, we investigated heterogeneous photochemical reactions

17 of SO_2 on five mineral oxides (SiO_2, kaolinite, Al_2O_3, MgO, and CaO) without photocatalytic

18 activity. Light significantly enhanced the uptake of SO_2, and its enhancement effects negatively

19 depended on the basicity of mineral oxides. The initial uptake coefficient ($\gamma_{0,\,BET}$) and the

20 steady-state uptake coefficient ($\gamma_{s,\,BET}$) of SO_2 positively relied on light intensity, relative

21 humidity (RH) and O_2 content, while they exhibited a negative relationship with the initial SO_2

22 concentration. Rapid sulfate formation during photo-induced heterogeneous reactions of SO_2

23 with all mineral oxides was confirmed to be ubiquitous, and H_2O and O_2 played key roles in

24 the conversion of SO_2 to sulfates. Specially, triplet states of SO_2 ($^3SO_2$) were suggested to be

25 the trigger for photochemical sulfate formation. Atmospheric implications supported a

26 potential contribution of interfacial SO_2 photochemistry on non-photoactive mineral dust to

27 atmospheric sulfate sources.

29   **Keywords:** SO_2; Sulfates; Non-photoactive mineral dust; Heterogeneous photochemistry

28

30

31

32   **1 Introduction**

33   As an important trace gas in the atmosphere, SO_2 is mainly emitted by volcanic eruption and

34   fuel combustion. There is an uneven distribution of atmospheric SO_2 concentrations that show

35   a distinctive seasonal and regional differentiation. Typical mixing ratios of SO_2 in the

36   troposphere are below 0.5 ppb for clean weather days, rising to several hundred ppb during

37   polluted days in urban regions (Ma et al., 2020). About half of SO_2 is oxidized to sulfate (He

38   et al., 2012), which is a key component of fine particulates in the atmosphere. High sulfate

39   loading in $PM_{2.5}$ was observed (Shao et al., 2019), especially in polluted regions where high-

40   sulfur fuels are usually used (Olson et al., 2021). They significantly alter physicochemical

41   properties of aerosols in terms of hygroscopicity, acidity and light absorption (Chan and Chan,

42   2003; Cao et al., 2013; Lim et al., 2018). Sulfates may lead to negative health outcomes, such

43   as respiratory illness and cardiovascular (Shiraiwa et al., 2017). In addition, the deposition of

44   sulfates leads to adverse effects on ecosystems via the acidification of soils and lakes

45   (Golobokova et al., 2020). Therefore, the oxidation of SO_2 to form sulfates has attracted

46   widespread attention in the past decades.

47   The conversion of SO_2 to sulfates in the atmosphere usually occurs in different phases: gas-

48   phase oxidation of SO_2 by hydroxyl radicals (•OH) or Criegee intermediate radicals (Mauldin

49   et al., 2012; Davis et al., 1979); aqueous-phase reaction of SO_2 with O_3, peroxides or transition

50   metal ions dissolved in cloud and fog droplets (Alexander et al., 2009; Herrmann et al., 2000;

51   Harris et al., 2013; Liu et al., 2020a; Li et al., 2020); and heterogeneous SO_2 uptake on aerosols

52   including authentic mineral dust, soot, inorganic ion and organic compounds (Adams et al.,

53   2005; He et al., 2018a; Ye et al., 2018; Wang et al., 2019; Yao et al., 2019; Zhang et al., 2020a;

54   Liu et al., 2020; Liu et al., 2021). However, the oxidation of SO_2 in gas and aqueous phases

55   fails to explain high sulfate concentrations in the polluted areas. Model simulation suggests

56 that the rapid sulfate formation can be attributed to the heterogeneous SO_2 uptake (Li et al.,

57 2017). A positive relationship between the fraction of sulfates and mineral dust in haze days

58 has been reported, implying that mineral dust may account for the formation of sulfates (Wang

59 et al., 2020a). Moreover, a large amount of sulfates was observed to be formed on the surface

60 of mineral dust after long-distance transport (Prospero, 1999). Thus, investigating the

61 heterogeneous oxidation of SO_2 on mineral dust can provide basic data for the model

62 calculation to evaluate atmospheric sulfates.

63 Mineral dust, as the dominant component of particulate matters in the atmosphere, accounts

64 for about 30%−60% mass fractions of global aerosols (Dentener et al., 1996; Peng et al., 2012).

65 It primarily contains SiO_2 (40%−80%), followed by Al_2O_3 (10%−15%), Fe_2O_3 (6%−13%),

66 CaO (3%−10%), MgO (1%−7%) and TiO_2 (0.1%−5%) (Urupina et al., 2021; Urupina et al.,

67 2019; Usher et al., 2003). Mineral dust can provide active sites for the adsorption and reaction

68 of gases. Up to now, the heterogeneous SO_2 uptake on authentic mineral aerosols and model

69 mineral oxides has been widely reported (Ma et al., 2019; Goodman et al., 2001; Wang et al.,

70 2018; Wang et al., 2020b), with the uptake coefficient (γ) of SO_2 varying from 10^{-9} to 10^{-4}

71 (Urupina et al., 2019; Usher et al., 2002).

72 It was recognized that light could significantly enhance the heterogeneous conversion of SO_2

73 to sulfates on the surface of photocatalytic mineral dust (Chen et al., 2021; Li et al., 2019; Wang

74 et al., 2020b). Electron-hole pairs are produced via photo-induced electrons from the valence

75 band to the conduction band of photocatalytic metal oxides, and then react with H_2O and O_2 to

76 generate reactive oxygen species (ROS), such as •OH and •O_2^- (Chu et al., 2019). Sulfates are

77 produced by the heterogeneous reactions of SO_2 with ROS (Park and Jang, 2016; Park et al.,

78 2017; Langhammer et al., 2020; Bounechada et al., 2017). In particular, due to the large

79 abundance of non-photoactive mineral dust (more than 85% mass of total mineral dust in the

80 atmosphere) (Usher et al., 2003; Liu et al., 2022), revealing the photooxidation processes of

81 SO_2 on these mineral dust is of great importance to better reevaluate the sulfate formation on

82 aerosols in the global scale.

83 Hence, photochemical SO_2 uptake and sulfate formation on non-photoactive mineral oxides

were investigated using a flow reactor and an *in situ* diffuse reflectance infrared Fourier transform spectroscopy (DRIFTS). The SO_2 conversion to sulfates was examined under various conditions, and the roles of light intensity, SO_2 concentration, H_2O, O_2 and basicity of mineral oxides were determined. Reaction mechanisms and atmospheric implications were proposed, highlighting an important pathway accounting for the photochemical uptake of SO_2 to form sulfates on the non-photoactive surfaces.

2 Experimental methods

2.1 Materials

Analytical grade SiO_2 (Sinopharm Chemical Reagent Co., Ltd.), kaolinite (Sinopharm Chemical Reagent Co., Ltd.), Al_2O_3 (Alfa Aesar), MgO (Sigma-Aldrich), and CaO (Sigma-Aldrich) were used in the experiments. Through the nitrogen Brunauer-Emmett-Teller (BET) physisorption analysis, their specific surface areas were detected to be 0.419, 6.407, 8.137, 10.948 and 6.944 $m^2\,g^{-1}$, respectively. With $BaSO_4$ used as the reference, the ultraviolet-visible (UV-vis) light absorption spectra of samples (Figure S1) in the wavelength range of 300–800 nm were obtained by the Shimadzu UV-2550 spectrophotometer, which was equipped with diffuse reflection integrating sphere attachment. The solid powder (0.2−5 g) was uniformly dispersed into 10.0 mL ethanol solution. The mixed liquid was poured into a rectangle quartz sample dish (14.0 cm × 7.0 cm) and dried to form a solid coating in an oven at 353 K for 10 h. SO_2 standard gas (50 ppm in N_2, Shenyang Air Liquide Co., LTD) and high purity N_2 and O_2 (99.999 vol.%, Shenyang Air Liquide Co., LTD) were used as received. The solid sample powder (0.2 g) was immersed in 10 mL deionized water (20 $mg\,mL^{-1}$), and then the suspension was vigorously stirred for 10 min. The pH of SiO_2, kaolinite, Al_2O_3, MgO and CaO suspension was measured to be 6.27, 6.58, 9.33, 10.61 and 12.72 using a pH meter, respectively.

2.2 Rectangular flow reactor

The uptake experiments of SO_2 on mineral dust were performed in a horizontal rectangular flow reactor (26.0 cm length × 7.5 cm width × 2.0 cm height), which was depicted in Figure S2. In a previous study, a similar rectangular flow reactor was designed and the feasibility of

112   the reactor has been verified (Knopf et al., 2007). The reactor was made of quartz to allow the

113   transmission of light. The temperature was maintained at 298 K by circulating temperature-

114   controlled water through the outer jacket of the reactor. Synthetic air with a N_2/O_2 volume ratio

115   of 4:1 was introduced into the flow reactor, and its total flow rate was 1000 mL min^{-1}. The

116   Reynolds number (*Re*) was calculated to be 28.2 (*Re* < 200), as described in the Supporting

117   Information, indicating a laminar flow state. SO_2 together with high purity N_2 (100 mL min^{-1})

118   was introduced into the reactor through a movable T-shaped injector equipped with six exit

119   holes (0.2 mm diameter), so that the gas could be uniformly distributed over the width of the

120   reactor. The SO_2 concentration was 40−200 ppb and measured with a SO_2 analyzer (Thermo

121   43i). Wet N_2 generated with a bubbler containing deionized water was introduced by two

122   parallel inlets on the side of a T-shaped injector. Relative humidity (RH, 10%−75%) was

123   controlled by regulating the ratio of dry N_2 to wet N_2 and measured via a hygrometer (Center

124   314). The equivalent layer numbers of water on surface was 0.9−4.0 according to the Brunauer-

125   Emmett-Teller (BET) model (Sumner et al., 2004), and the thickness of the film of adsorbed

126   water varied between 2.7−12 nm at RH=10%−75%. There were three equally spaced exhaust

127   ports to mitigate the outlet turbulence. A xenon lamp (CEL-LAX500, China Education Au-light

128   Co., Ltd) was used to simulate sunlight and vertically located above the reactor. A filter was

129   placed on the reactor to remove the light with wavelengths shorter than 300 nm. The spectrum

130   irradiance of the xenon lamp was displayed in Figure S3 and measured using a calibrated

131   spectroradiometer (ULS2048CL-EVO, Avantes). The spectral irradiance was measured inside

132   the reactor, after passing the water cooling and in the absence of a sample. The total irradiance

133   ($0-7.93 \times 10^{16}$ photons cm^{-2} s^{-1}) on the coating can be adjusted by varying the distance of the

134   xenon lamp to the reactor.

135   **2.3 Uptake coefficient of SO_2**

136   The heterogeneous reaction kinetics of SO_2 with mineral dust can be described by a pseudo-

137   first-order reaction. Figure S4 showed a linear relationship between the natural logarithm of

138   the SO_2 concentration and the reaction time. The apparent rate constant (k_{obs, SiO_2}) of SO_2 with

139   SiO_2 can be calculated using equation 1,

140 $$\frac{\ln(C_0/C_t)}{t} = k_{obs, SiO_2} \quad (1)$$

141 where C_0 and C_t (ppb) are the initial SO_2 concentration and the SO_2 concentration, respectively;

142 t was calculated by diving the length of the reactive surface by the average flow velocity. The

143 loss of SO_2 on the internal wall of the reactor in blank experiments was carried out under

144 various conditions (Figure S5 as an example), and it has been deducted for the γ calculation.

145 Assuming that the wall loss was constant in the experiments with and without samples, the

146 geometric uptake coefficient (γ_{geo}) was determined by equation 2 (Knopf et al., 2007),

147 $$\gamma_{geo} = \frac{4Vk}{S\omega} \quad (2)$$

148 where k (s^{-1}), V (4×10^{-4} m^3), S (9.8×10^{-3} m^2) and ω (314.05 m s^{-1}) are the reaction rate

149 constant, the volume of the rectangular reactor, the surface area of the sample dish, and the

150 mean molecular speed of SO_2, respectively.

151   The uptake process of SO_2 on SiO_2 depended on the reaction of SO_2 with SiO_2 and the mass

152 transport of SO_2 to the surface. It can be expressed by equation 3,

153 $$k'_{r, SiO_2} = \left[\frac{1}{k_{obs, SiO_2} - k_{obs, wall}} - \frac{a}{N_u D}\right]^{-1} \quad (3)$$

154 where k_{obs, SiO_2} and $k_{obs, wall}$ (s^{-1}) are the apparent rate constants measured with and without

155 SiO_2 samples, respectively. k'_{r, SiO_2} is the reaction rate constant of SO_2 accounting for the

156 diffusion effect; D (0.1337 cm^2 s^{-1}) is the diffusion coefficient of SO_2 in air; a (1 cm) is one

157 half height of the flow reactor; N_u is the Nusselt numbers obtained with a calculation method

158 from Solbrig and Gidaspow (1967), which represents the mass transport. Then, the corrected γ

159 can be calculated by equation 2 where k was replaced by k'_{r, SiO_2}. In our experiments, the

160 correction for γ was estimated to be 10%. Initial uptake coefficients (γ_0) and steady-state uptake

161 coefficients (γ_s) were calculated by averaging the signals within the 1.0 and 40−60 min reaction

162 time, respectively.

163   To understand the diffusion depth of SO_2 and determine the interaction of SO_2 with the

164 underlying layers of SiO_2, the uptake of SO_2 as a function of the SiO_2 mass under irradiation

165 was shown in Figure S6. The γ exhibited a linear increase in the SiO_2 mass range of 0.05−2.0

166 g, while it remained unchanged at the SiO₂ mass > 3.0 g. Therefore, the uptake coefficient of

167 SO₂ in the linear regions was normalized using the BET surface area of SiO₂ by equation 4

168 (Brunauer et al., 1938),

169 $\gamma_{\text{BET}} = \dfrac{S_{\text{geo}} \times \gamma_{\text{geo}}}{S_{\text{BET}} \times m_{\text{SiO}_2}}$ (4)

170 where γ_{BET} is the SO₂ uptake coefficient normalized to the BET surface area; S_{geo} (9.8×10^{-3}

171 m²) is the geometric area of the sample dish; S_{BET} (0.419 m² g⁻¹) is the BET surface area of

172 SiO₂; m_{SiO_2} (0.05−2.0 g) is the SiO₂ mass. The same method was also used to calculate the

173 uptake coefficients of SO₂ on other mineral oxides.

2.4 In Situ DRIFTS analysis

175   The changes in the chemical compositions on mineral oxides in the SO₂ uptake process were

176 investigated by the Fourier transform infrared (FTIR) spectrometer (Thermo Nicolet iS50)

177 equipped with an *in situ* diffuse reflectance accessory and a mercury cadmium telluride (MCT)

178 detector. About 14 mg mineral oxides were placed into a stainless-steel cup inside the reaction

179 cell. To remove adsorbed impurities, SiO₂ was purged with a 150 mL min⁻¹ airflow (N₂/O₂

180 volume ratio = 4:1) at RH=40% for 1 h. Then, a background spectrum of unreacted samples

181 was collected. SO₂ (2 ppm) was introduced into the reaction cell, and the IR spectra was

182 recorded as a function of time at a resolution of 4 cm⁻¹ by averaging 100 scans. The light from

183 the xenon lamp (500 W) was transmitted into the DRIFTS reaction cell via a fiber. To verify

184 the role of intermediate, Ru(bpy)₃(Cl)₂) and NaHCO₃, acting as ³SO₂ and •OH scavengers

185 (Bulgakov and Safonova, 1996; Gen et al., 2019a), respectively, were mixed with SiO₂ powder

186 in an agate mortar, and the mixture was put in the reaction cell of DRIFTS.

187

3 Results and discussion

3.1 Photo-enhanced uptake of SO₂

190   Acting as the most abundant mineral oxides, SiO₂ was firstly used to investigate the uptake

191 behaviors of SO₂. As shown in Figure 1A, when SO₂ (80 ppb) was exposed to SiO₂ in the dark,

192 the SO₂ concentration decreased to 70 ppb, and then it quickly increased and reached a steady

state after 20 min. Upon exposure to SiO_2 under irradiation, the SO_2 concentration exhibited a greater drop than that in the dark. The deactivation of SO_2 uptake on SiO_2 was very slight after 20 mins under irradiation. These suggest that light can significantly promote the heterogeneous reaction of SO_2 on SiO_2. Few studies observed the photochemical uptake of SO_2 on non-photoactive minerals (Xu et al., 2021; Zhang et al., 2022). When SO_2 did not contact with SiO_2, its concentration recovered rapidly. The desorption of SO_2 was observed when SO_2 was isolated from SiO_2 in the dark and under irradiation, indicating that the physical adsorption partially contributed to the SO_2 loss during the photochemical process. The proportion of the desorbed SO_2 during the uptake process can be quantified by dividing the integral of reversible desorption of SO_2 ($t = 80$–100 min) into the integral of the SO_2 uptake ($t = 20$–80 min), which was calculated to be 95% and 12% in the dark and under irradiation, respectively. This implies that SO_2 uptake in the dark was primarily ascribed to the physical adsorption of SO_2, while SO_2 uptake under irradiation was mainly attributed to chemical processes or irreversible adsorption.

The uptake coefficients of SO_2 on SiO_2 as a function of irradiation intensity were shown in Figure 1B. The errors in all figures are the standard deviations of three repetitive experiments. Both $\gamma_{0,\,BET}$ and $\gamma_{s,\,BET}$ displayed a well linear relationship with the irradiation intensity, further confirming the photochemical nature of the reactions of SO_2 on SiO_2. In particular, $\gamma_{0,\,BET}$ and $\gamma_{s,\,BET}$ on SiO_2 under simulated solar irradiation was comparable with those (10^{-7}–10^{-6}) on Gobi Desert dust (GDD) and Arizona Test Dust (ATD) under UV irradiation, which contained photocatalytic metal oxides (Park et al., 2017). As for the SO_2 uptake on TiO_2, $\gamma_{0,\,BET}$ and $\gamma_{s,\,BET}$ were measured to be 10^{-6} and 10^{-7}, respectively, by using the flow tube (Ma et al., 2019), which were similar to our results. It should be pointed out that the similar uptake coefficient did not mean the comparable ability of photoactive and non-photoactive mineral oxides to SO_2 uptake, since the uptake coefficient was highly dependent on environmental conditions (SO_2 concentration, relative humidity, mineral oxides mass, light source and pressure) and reactor type (chamber and flow tube reactor). Table S1 shows that the fraction of SiO_2 in the sample was 99.02%, accompanied by a small amount of Al_2O_3, K_2O, Fe_2O_3 and CaO. Photoactive

220   substances (Fe_2O_3) was very few in the sample, and they should not be the main contributor to

221   the photochemical uptake of SO_2.

222   Figure 1C shows the evolution of $\gamma_{0,\,BET}$ and $\gamma_{s,\,BET}$ at different SO_2 concentrations under

223   irradiation. An inverse dependence of $\gamma_{0,\,BET}$ and $\gamma_{s,\,BET}$ on the SO_2 concentration was observed,

224   meaning that the efficiency of SO_2 uptake decreased with increasing the SO_2 concentration.

225   The uptake of gases on the solid surfaces usually follows the Langmuir-Hinshelwood (L-H)

226   mechanism (Ammann et al., 2003; Zhang et al., 2020b), suggesting that gaseous molecules are

227   quickly absorbed on the surfaces, and then the reactions occur among the absorbed species.

228   Assuming that the adsorption of SO_2 on SiO_2 is in accord with the Langmuir isotherm, the

229   dependence of γ on the SO_2 concentration can be described by equation 5 (Zhang et al., 2020b),

230      $$\gamma = \frac{(4V/S\omega)k[SiO_2]_T K_{SO_2}}{1 + K_{SO_2}[SO_2]_g} \quad (5)$$

231   where $[SO_2]_g$ is the concentration of gaseous SO_2; $[SiO_2]_T$ is the total number of active sites

232   on SiO_2; k is the reaction rate constant of SO_2 absorbed on SiO_2; K_{SO_2} represents the Langmuir

233   adsorption constant of SO_2. Because the SiO_2 mass remained constant during the reaction,

234   equation 5 can be written as equation 6,

235      $$\gamma = \frac{a}{1 + K_{SO_2}[SO_2]_g} \quad (6)$$

236   where $a = (4V/S\omega)k[SiO_2]K_{SO_2}$. As shown in Figure 1C, equation 6 can well describe the

237   correlation of the SO_2 uptake coefficient with the SO_2 concentration, suggesting that the L-H

238   mechanism can explain the influence of the SO_2 concentration on $\gamma_{0,\,BET}$ and $\gamma_{s,\,BET}$.

239
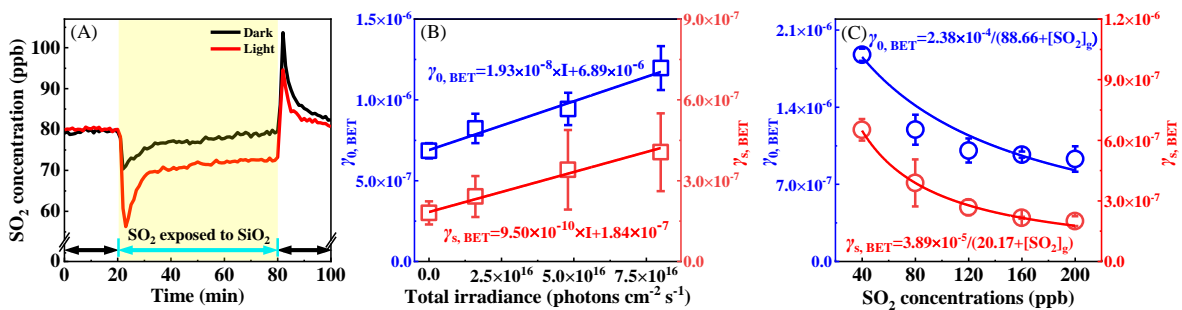
240   **Figure 1.** (A) The temporal variation of the SO_2 concentration on SiO_2 in the dark and under

241   irradiation (7.93×10^{16} photons cm^{-2} s^{-1}); The background changes of the SO_2 concentration

242 in the blank reactor have been deducted. (B) The $\gamma_{0,\text{BET}}$ and $\gamma_{s,\text{BET}}$ of SO_2 on SiO_2 as a

243 function of the light intensity. (C) The $\gamma_{0,\text{BET}}$ and $\gamma_{s,\text{BET}}$ of SO_2 on SiO_2 at different SO_2

244 concentrations under irradiation (7.93×10^{16} photons cm^{-2} s^{-1}); The fitting lines for $\gamma_{0,\text{BET}}$

245 and $\gamma_{s,\text{BET}}$ were based on the Langmuir-Hinshelwood mechanism using equation 6. Reaction

246 conditions: SiO_2 mass of 0.2 g, temperature of 298 K, RH of 40% and O_2 content of 20%.

247 **3.2 Photo-induced formation of sulfates by the SO_2 uptake**

248 To investigate the products formed on SiO_2, *in situ* DRIFTS spectra were recorded, as shown

249 in Figure 2. The band at 1359 cm^{-1} was assigned to physically-adsorbed SO_2 on SiO_2 (Urupina

250 et al., 2019). The bidentate sulfate and bisulfate contributed to the bands at 1260 and 1229/1074

251 cm^{-1} (Urupina et al., 2019; Yang et al., 2020), respectively. The bands at 1038 cm^{-1} may be

252 related to the monodentate sulfite (Yang et al., 2019; Wang et al., 2019). It was noted that the

253 intensity of physically-absorbed SO_2 (1359 cm^{-1}) under irradiation was lower than that in the

254 dark (Figure S7), which may be ascribed to further conversion of SO_2 absorbed on SiO_2 under

255 irradiation. Especially, the sulfate bands (1260, 1229 and 1074 cm^{-1}) only appeared under

256 irradiation, while the sulfites (1038 cm^{-1}) were only detected in the dark. This suggests that

257 light changed the SO_2 conversion pathways on SiO_2. As shown in Figure S7, the bands at

258 1157/1055 cm^{-1} were assigned to the asymmetric stretching of Si−O (Hu et al., 2003). Sulfate

259 generated on the surface may interact with SiO_2, leading to a decrease in the intensity of peaks

260 (1157/1055 cm^{-1}).

261
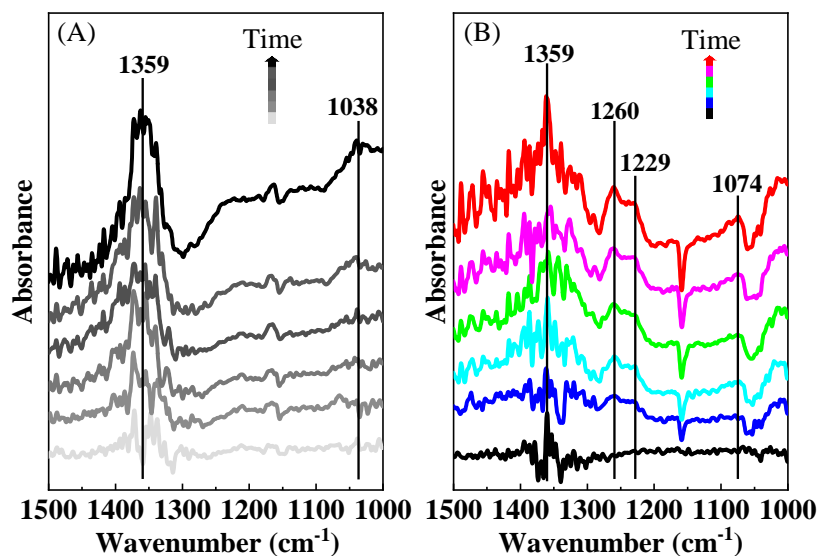
Figure 2. *In situ* DRIFTS spectra of SiO_2 during the uptake process of SO_2 (2 ppm) in the dark (A) and under irradiation (B). Reaction conditions: RH of 40%, temperature of 298 K and O_2 content of 20%.

3.3 Key roles of H_2O and O_2 in photochemical conversion of SO_2 to sulfates

Figure S8A shows temporal variations of the SO_2 concentration in the reaction with SiO_2 at RH=10% and 60% under irradiation. The uptake of SO_2 was very weak at RH=10%, whereas it was obvious at RH=60%. Moreover, H_2O markedly prolonged the time to reach the steady-state uptake of SO_2. This means that H_2O plays an enhancement role in the photochemical uptake of SO_2. As shown in Figure 3A, $\gamma_{0,\,BET}$ had a continuous increase from $(1.20 \pm 0.04) \times 10^{-7}$ to $(1.54 \pm 0.07) \times 10^{-6}$ with increasing the RH in the 10%−60% range, but it decreased to $(1.05 \pm 0.09) \times 10^{-6}$ at RH=75%. The $\gamma_{s,\,BET}$ linearly depended on the RH, and linear fitting to $\gamma_{s,\,BET}$ versus RH yielded an equation $\gamma_{s,\,BET} = 1.31 \times 10^{-8} \times RH - 1.02 \times 10^{-7}$. Adsorbed H_2O promoted the hydration and dissociation of SO_2 (Huang et al., 2015), and it may generate reactive oxygen species (ROS) such as $\bullet OH$ or HO_2 radicals to oxidize SO_2 under irradiation (Li et al., 2020; Ma et al., 2019), which would lead to positive effects of RH on the SO_2 uptake. Adsorbed H_2O also occupied adsorptive and active sites on the surface, leading to a decrease in SO_2 adsorption. When this competitive role was dominated, the uptake of SO_2 would be

279   hindered.

280   The DRIFTS spectra of SiO_2 during the SO_2 uptake at different RHs are shown in Figure

281   S9A. The band intensities of sulfates (1260 and 1229 cm^{-1}) at RH=60% were stronger than

282   those at RH=10%, suggesting that H_2O significantly promotes the sulfate formation. To further

283   investigate the influence of H_2O on the sulfate formation, the integrated area of sulfates in the

284   DRIFTS spectra (1289−1202 cm^{-1}) as a function of the time at different RHs is illustrated in

285   Figure 3B. Sulfates exhibited a fast formation in the initial 30 min, and then they were

286   continuously generated at a relatively slow rate. SO_2 absorption on the surface would be

287   blocked because of the accumulation of H_2O and products (sulfites and sulfates), resulting in

288   the gradual deactivation of the surface. It was noted that sulfates formation was more prominent

289   at higher RH, revealing that H_2O can act as an important participator in the production of

290   sulfates by the photochemical uptake of SO_2 on SiO_2.
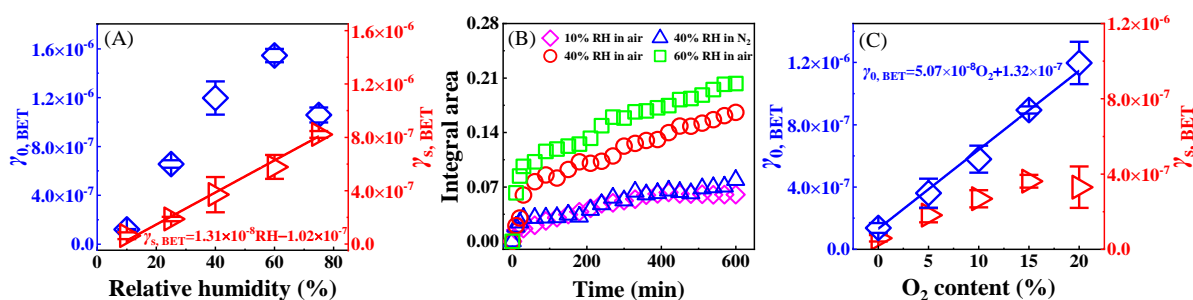
291

292   **Figure 3.** (A) The dependence of $\gamma_{0,\,BET}$ and $\gamma_{s,\,BET}$ on RH. (B) Integrated area of sulfates in

293   DRIFTS spectra (1289−1202 cm^{-1}) as a function of time. (C) The dependence of $\gamma_{0,\,BET}$ and

294   $\gamma_{s,\,BET}$ on O_2. Reaction conditions: SiO_2 mass of 0.2 g, irradiation intensity of 7.93×10^{16}

295   photons $cm^{-2}\,s^{-1}$, temperature of 298 K, O_2 content of 20% for (A) and RH of 40% for (B).

296   Figure S8B displays effects of O_2 on the photochemical uptake of SO_2 on SiO_2. Negligible

297   SO_2 uptake occurred in N_2, while there was a significant decrease in the SO_2 concentration in

298   air. The $\gamma_{0,\,BET}$ greatly increased from $(1.37 \pm 0.45) \times 10^{-7}$ under anaerobic condition to (1.19

299   $\pm\ 0.13) \times 10^{-6}$ under 20% O_2 content condition (Figure 3C), confirming that O_2 was involved

300   in the reaction of SO_2 on SiO_2. The $\gamma_{s,\,BET}$ increased from $(7.10 \pm 2.85) \times 10^{-8}$ under anaerobic

301   condition to $(4.37 \pm 0.58) \times 10^{-7}$ under 15% O_2 content condition, whereas it remained

302   unchanged with further increasing the O_2 content.

303   DRIFTS spectra of SiO_2 during the SO_2 uptake in N_2 and air was compared in Figure S9B.

304   In both air and N_2, the bands of absorbed SO_2 (1359 cm^{-1}), sulfates (1260, 1229 and 1074

305   cm^{-1}). Nevertheless, their intensities in N_2 were weaker than those in air. According to the

306   integrated area of sulfates in the DRIFTS spectra (1289−1202 cm^{-1}), the formation trends of

307   sulfates were similar in N_2 and air (Figure 3B), while the sulfate formation rate in N_2 was

308   obviously lower than that in air, meaning that O_2 enhanced the sulfate production. It was

309   reported that the production rate of sulfates from the SO_2 uptake on TiO_2 and by the photolysis

310   of nitrates under UV irradiation in N_2 was also smaller than that in air (Ma et al., 2019; Gen et

311   al., 2019b). In addition, it was noted that sulfates can be generated in N_2, meaning that O_2 was

312   not necessary and some pathways contributed to sulfates without O_2.

313   **3.4 Ubiquitously photoenhanced conversion of SO_2 to sulfates**

314   To better assess the potential for photochemical conversion of SO_2 to sulfates, the SO_2 uptake

315   experiments were further performed on typical mineral oxides without photocatalytic activity.

316   As displayed in Figure S10, more obvious SO_2 uptake on kaolinite, Al_2O_3, MgO and CaO were

317   observed under irradiation compared to those in the dark. Figure 4A shows that there was the

318   largest $\gamma_{s,\,BET}$ for CaO among five minerals, and $\gamma_{s,\,BET}$ positively depended on the basicity (pH)

319   of mineral oxides. Basic oxides generally contains more surface hydroxyls, which enhanced

320   the heterogeneous uptake of SO_2 (Zhang et al., 2006). The ratios of steady-state uptake

321   coefficients under irradiation to those in the dark ($\gamma_{s,\,Light}/\gamma_{s,\,Dark}$) were larger than 1.0 for all

322   mineral oxides (Figure 4B). The experiments for the pH dependence on SiO_2 have been also

323   performed (Figure S11). The pH of SiO_2 suspension was adjusted to pH = 9, and $\gamma_{s,\,BET}$ and

324   $\gamma_{s,\,Light}/\gamma_{s,\,Dark}$ were determined to be $(8.79 \pm 0.85) \times 10^{-6}$ and 1.31, respectively (Figure 4A and

325   4B). These results suggest that light can generally enhance the SO_2 uptake on minerals at a

326 wide pH range. However, the $\gamma_{Light}/\gamma_{Dark}$ had smaller values with an increase in the basicity,

327 suggesting that the promotion effect of the light was less remarkable for basic oxides.
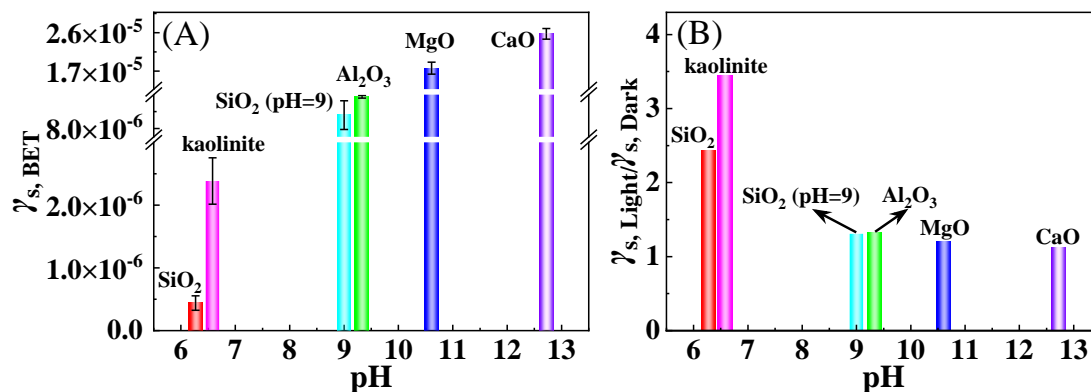
329 **Figure 4.** (A) The dependence of $\gamma_{s, BET}$ under irradiation on the basicity (pH) of mineral

330 oxides. (B) The ratios of steady-state uptake coefficients under irradiation to those in the dark

331 ($\gamma_{s, Light}/\gamma_{s, Dark}$). Reaction conditions: mineral oxides mass of 0.2 g, irradiation intensity of

332 7.93×10^{16} photons cm^{-2} s^{-1}, temperature of 298 K, RH of 40% and O_2 content of 20%.

333 As shown in Figure 5A and B, the band at 1300 cm^{-1} should be ascribed to the sulfate. The

334 intensity of sulfate (1300 and 1220 cm^{-1}) under irradiation was larger than those in the dark.

335 Compared to weaker peaks of sulfates (1200 and 1260 cm^{-1}) for Al_2O_3 in the dark (Figure 5C),

336 a stronger band of bisulfates appeared at 1220 cm^{-1} under irradiation (Figure 5D). By contrast

337 to the generation of sulfates for kaolinite and Al_2O_3, both sulfites and sulfates formations were

338 observed for MgO and CaO (Figure 5E−H). Sulfites were dominant in the dark, as shown by

339 the peaks at 966 and 1020 cm^{-1} for MgO and 943 cm^{-1} for CaO, whereas the sulfate formation

340 was significantly enhanced under irradiation according to peak intensities at 1163 cm^{-1} for

341 MgO and 1137 cm^{-1} for CaO. It should be noted that these mineral oxides were non-

342 photoactive because of their poor light absorption property (Figure S1). Nevertheless, the light

343 can greatly promote the formation of sulfates via the SO_2 uptake process on mineral oxides

344 without photocatalytic activity.
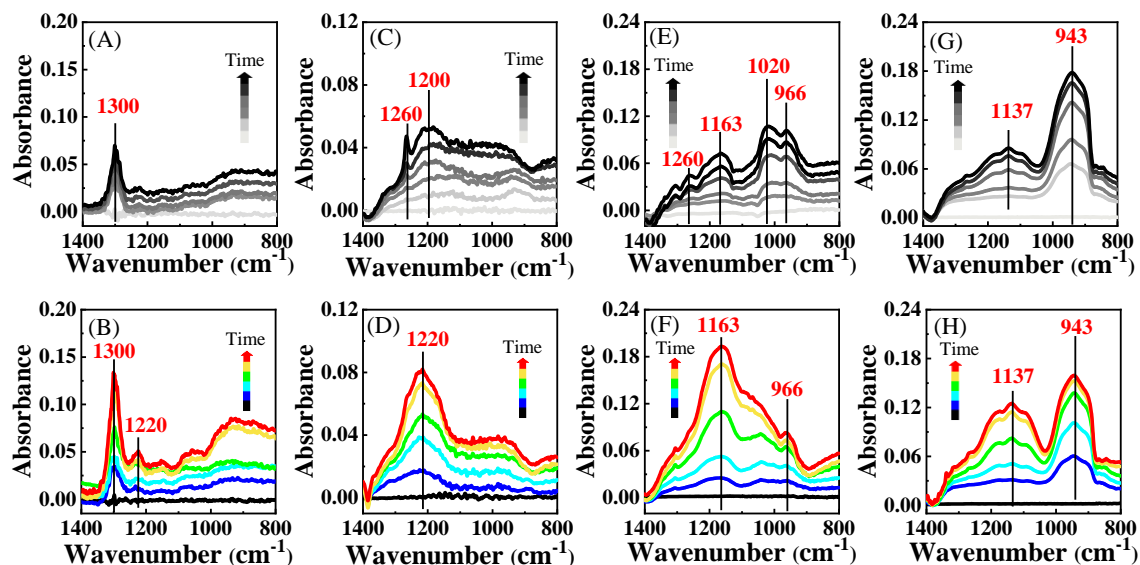
345

346 **Figure 5.** *In situ* DRIFTS spectra of kaolinite (A and B), Al₂O₃ (C and D), MgO (E and F),

347 CaO (G and H) during the uptake process of SO₂ (2 ppm) for 600 min in the dark (black

348 lines) and under irradiation (colorful lines). Reaction conditions: RH of 40%, temperature of

349 298 K and O₂ content of 20%.

3.5 Conversion mechanisms of SO₂ to sulfates

351 Heterogeneous photochemical reaction mechanisms of SO_2 on non-photoactive mineral dust

352 were proposed in light of experimental observations (Figure 6). Gaseous SO_2 was adsorbed on

353 the surface (R1), and then reacted with H_2O to form sulfites (R2). Under irradiation, adsorbed

354 SO_2 accepted photons to form its singlet states ($^1SO_2$) and $^3SO_2$ (R3−5) (Sidebottom et al., 1972;

355 Martins-Costa et al., 2018). The reaction between $^3SO_2$ and H_2O resulted in the formation of

356 HOSO• and •OH (R6), which can combine with SO_2 to produce $HOSO_2$• (R7). HOSO• and

357 $HOSO_2$• can be transformed into SO_3, which reacted with H_2O to drive the sulfate formation

358 (R8 and R9). The interaction between $^3SO_2$ and O_2 may also generate SO_3 directly, which

359 would be converted to sulfates subsequently (R10). Theoretical calculations suggested that the

360 multistep reactions between $^3SO_2$ with H_2O and O_2 had small energy barriers or were barrier-

361 free (Gong et al., 2022), which could enhance the generation of ROS and the transformation of

362 S(IV) to S(VI). As displayed by R11 and R12, SO_2 and H_2SO_3 adsorbed on the surface may be

363 oxidized to form sulfates via the reactions with ROS including •O, •OH or HO_2• , which were

364 produced in R6 and R8−10. In addition, gaseous SO_2 could be dissolved into adsorbed H_2O to

365 generate bisulfites, which would be finally converted to sulfates by ROS (R13) (Urupina et al.,

366 2019). As displayed in Figure S12A, the IR peaks of sulfates were not observed when tris (2,2′-

367 bipyridine) ruthenium dihydrochloride ($Ru(bpy)_3(Cl)_2$) was employed as the quencher of $^3SO_2$.

368 The peaks were assigned to the vibrations of excited $Ru(bpy)_3(Cl)_2$ (Mukuta et al., 2014). This

369 definitely proves that $^3SO_2$ is the key trigger for the sulfate formation. Figure S12B shows that

370 the peaks of sulfates were obviously weaker in the presence of $NaHCO_3$, confirming the

371 dominant contribution of •OH formed in R6 and R9 to the formation of sulfates.

372   Several photochemical mechanisms have been reported to explain the sulfate formation via

373 the SO_2 uptake on various surfaces. Photoactive mineral oxides (such as TiO_2, F_2O_3 and ZnO)

374 can accept photons to produce electron-hole pairs, which generated ROS for the conversion of

375 SO_2 to sulfates (Ma et al., 2019; Li et al., 2019; Wang et al., 2020b). For example, •OH and

376 HO_2•, generated from the reaction of hole with H_2O and electron with O_2, respectively, can act

377 as oxidizing agents for the reaction with SO_2 (Ma et al., 2019). Similarly, the reaction of SO_2

378 with photo-induced •OH obviously enhanced the formation of sulfate on diesel soot and actual

379 $PM_{2.5}$ (Zhang et al., 2022; Zhang et al., 2020c). NO_2 and NO_2^-/HNO_2 can be formed in the

380 nitrates photolysis, and primarily contributed to the oxidation of SO_2 to sulfates on nitrates (Gen

381 et al., 2019b; Gen et al., 2019a). Theoretically, the mechanism proposed in this study should

382 also occur on photo-excited substrates. Taking TiO_2 as an example, SO_2 competed with TiO_2

383 for photons, and the production efficiency of $^3SO_2$ and excited state of TiO_2 (TiO_2*) depended

384 on their light absorption properties. Meanwhile, $^3SO_2$ had a competition electron-hole pairs

385 generated from TiO_2* for O_2 and H_2O. Thus, the dominant mechanism for the SO_2 uptake on

386 TiO_2 should be related to light absorption properties of precursors and the reactivity for $^3SO_2$

387 and TiO_2* to O_2 and H_2O. By contrast, all mineral oxides used here cannot be excited under

388 irradiation according to their light absorption spectra (Figure S1). Nevertheless, SO_2 adsorbed

389 on mineral oxides can absorb the ultraviolet radiation (290−400 nm) to form the excited states

390 of SO_2 (SO_2^*) (Kroll et al., 2018), which subsequently reacted with H_2O and O_2, finally

391 converting SO_2 to sulfates. The SO_2 uptake experiment in the dark and the visible light (>420

392   nm) was carried out (Figure S13). An ignorable difference was observed for the SO_2

393   concentration with or without visible light, suggesting that visible light had a minor contribution

394   to the photoenhanced SO_2 uptake.

395   According to the experimental results, some surfaces, providing absorptive sites for SO_2, can

396   enhance the photooxidation of SO_2 to sulfates. However, the promotion effect would vary with

397   different substances. For example, the current experiments on some basic minerals indicate that

398   light plays a minor enhancement role in the SO_2 uptake (Figure 4), but it could still enhance the

399   sulfate formation (Figure 5). The solubility and effective Henry's law constant of SO_2 were

400   positively dependent on pH. Thus, SO_2 was more liable to be dissolved to form HSO_3^-/SO_3^{2-}

401   on more alkaline surface, leading to a strong SO_2 uptake in the dark (Figure 4A and 4B), and

402   abundant sulfites on surfaces (Figure 5). Nevertheless, gaseous SO_2 tends to be adsorbed on

403   kaolinite and Al_2O_3 due to less solubility of SO_2 on these surfaces, and then converted to sulfate

404   under irradiation (Figure 6). Accordingly, a strong promotion effect of light on SO_2 uptake was

405   observed on neutral and weakly alkaline surfaces (Figure 4B).
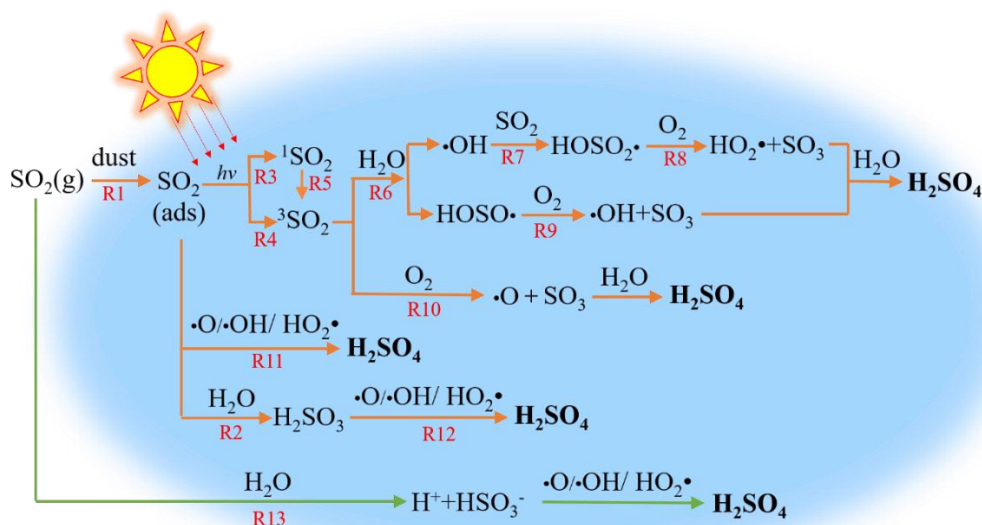
406

407   **Figure 6.** The proposed photochemical conversion mechanisms of SO_2 to sulfates on non-

408   photoactive mineral dust.

409   **4 Atmospheric implications**

410   The lifetime (τ) for photochemical loss of SO_2 on mineral dust was given using equation 7,

411 $$\tau = \frac{4}{\gamma \omega A} \quad (7)$$

412 where γ and ω are the uptake coefficient and the mean molecular speed of SO_2, respectively; A

413 is the surface area density of mineral dust, and it is estimated to be $(1.4\text{–}4.8) \times 10^{-5}$ cm^2 cm^{-3}

414 (Zhang et al.,2019; He et al., 2018b). In this work, $\gamma_{s,\,BET}$ of SO_2 on several mineral oxides

415 were measured to be $4.39 \times 10^{-7}\text{–}3.45 \times 10^{-5}$ (Reaction conditions: SO_2 concentration of 40

416 ppb, irradiation intensity of 7.93×10^{16} photons cm^{-2} s^{-1} and RH of 40%). Thus, the τ of SO_2

417 with respect to the photooxidation on mineral dust was calculated to be 0.9–240 days, which

418 was shorter than that (54 years) for the photochemical uptake of SO_2 on TiO_2 and the

419 corresponding one (346 days) for the heterogeneous oxidation of SO_2 on ATD in the presence

420 of nitrates (Ma et al., 2019; Zhang et al., 2019). The reaction conditions in this study and those

421 in the literatures are different in some respects, and the previously reported SO_2 uptake

422 coefficient $(10^{-7}\text{–}10^{-6})$ had a lower value (Ma et al., 2019). The huge difference in the τ of SO_2

423 was also ascribed to the variation in the surface area density. The content of TiO_2 in mineral

424 dust was only about 1%, and thus the surface area density of TiO_2 was about 10^{-7} cm^2 cm^{-3},

425 leading to a longer τ (54 years) for SO_2 on TiO_2 (Ma et al., 2019). It was comparable to the

426 lifetime (3.6−20 days) of SO_2 for the gas-phase reaction with •OH at a concentration of $\sim 10^{-6}$

427 molecules cm^{-3} (Huang et al., 2015; Zhang et al., 2019). Therefore, the photochemical process

428 with the excited state SO_2 acting as a driver on mineral dust was an important pathway for the

429 SO_2 sink in the atmosphere.

430 Sulfates show significant influences on the atmosphere, such as an important contributor to

431 the haze formation, affecting the activity of aerosols acting as cloud condensation nuclei (CCN)

432 and ice nuclei (IN), and modifying optical property and acidity of aerosols. A sulfate formation

433 rate (R) can be obtained using γ by equation 8 (Cheng et al., 2016),

434 $$R = \frac{d\left[SO_4^{2-}\right]}{dt} = \left[\frac{R_p}{D} + \frac{4}{\gamma \omega}\right]^{-1} A\left[SO_2\right] \quad (8)$$

435 where R_P is the radius of mineral dust, which can be estimated using equation 9 (Li et al., 2020),

436 $R_P = (0.254 \times [PM_{2.5}]/(\mu g\ m^{-3}) + 10.259) \times 10^{-9}$ m $\quad (9)$

where [PM$_{2.5}$] was average PM$_{2.5}$ mass concentration, and 300 μg m^{-3} was used for the polluted periods in typical China cities (Li et al., 2020; Guo et al., 2014). It was assumed that mineral dust accounted for 50% mass of PM$_{2.5}$ (Tohidi et al., 2022), and the mass fraction of SiO$_2$, Al$_2$O$_3$, MgO, and CaO in mineral dust was 60%, 12.5%, 4% and 6.5%, respectively (Urupina et al., 2021; Urupina et al., 2019; Usher et al., 2003). Thus, R was determined to be 2.15 μg m^{-3} h^{-1}. This suggests that the SO$_2$ uptake on non-photoactive surfaces may be an important sulfate formation pathway under irradiation in some dust-rich conditions.

Author contributions

CH, WY and JM designed and conducted experiments; CH, WY and JM analyzed the data and prepared the paper with contributions from HY; FL conducted experiments; CH supervised the project.

Competing interests

The authors declare that they have no conflict of interest.

Acknowledgements

This work was supported by the National Natural Science Foundation of China [grant number 42077198], the LiaoNing Revitalization Talents Program [grant number XLYC1907185], and the Fundamental Research Funds for the Central Universities [grant numbers N2325034; N2025011].

Reference

Adams, J., Rodriguez, D., and Cox, R.: The uptake of SO$_2$ on Saharan dust: A flow tube study, Atmos. Chem. Phys., 5, 2679-2689, https://doi.org/10.5194/acpd-5-2643-2005, 2005.

Alexander, B., Park, R. J., Jacob, D. J., and Gong, S.: Transition metal-catalyzed oxidation of atmospheric sulfur: Global implications for the sulfur budget, J. Geophy. Res., 114, 2309-2312, https://doi.org/10.1029/2008jd010486, 2009.

Ammann, M., Poschl, U., and Rudich, Y.: Effects of reversible adsorption and Langmuir-Hinshelwood surface reactions on gas uptake by atmospheric particles, Phys. Chem. Chem.

Phys., 5, 351-356, https://doi.org/10.1039/b208708a, 2003.

Bounechada, D., Anderson, D., Skoglundh, M., and Carlsson, P.: SO_2 adsorption on silica supported iridium, J. Chem. Phys., 146, 084701-084708, https://doi.org/10.1063/1.4976835, 2017.

Brunauer, B., Deming, L., Deming, W., and Teller, E.: Adsorption of gases in multimolecular layers, J. Am. Chem. Soc., 60, 309-319, https://doi.org/10.1021/ja01269a023, 1938.

Bulgakov, R. G. and Safonova, L. A.: Chemiluuminescence in the oxidation of Na_2S by oxygen in water solutions, Russ. Chem. Bull., 45, 1775-1776, https://doi.org/10.1007/bf01431827, 1996.

Cao, J., Tie, X., Dabberdt, W. F., Jie, T., Zhao, Z., An, Z., Shen, Z., and Feng, Y.: On the potential high acid deposition in northeastern China, J. Geophy. Res.: Atmos., 118, 4834-4846, https://doi.org/10.1002/jgrd.50381, 2013.

Chan, M. and Chan, C.: Hygroscopic properties of two model humic-like substances and their mixtures with inorganics of atmospheric importance, Environ. Sci. Technol. , 37, 5109-5115, https://doi.org/10.1021/es034272o, 2003.

Chen, Y., Tong, S., Li, W., Liu, Y., Tan, F., Ge, M., Xie, X., and Sun, J.: Photocatalytic oxidation of SO_2 by TiO_2: Aerosol formation and the key role of gaseous reactive oxygen species, Environ. Sci. Technol., 55, 9784-9793, https://doi.org/10.1021/acs.est.1c01608, 2021.

Cheng, Y., Zheng, G., Wei, C., Mu, Q., Zheng, B., Wang, Z., Gao, M., Zhang, Q., He, K., Carmichael, G., Pöschl, U., and Su, H.: Reactive nitrogen chemistry in aerosol water as a source of sulfate during haze events in China, Sci. Adv., 2, 1601530-1601540, https://doi.org/10.1126/sciadv.1601530, 2016.

Chu, B., Wang, Y. L., Yang, W. W., Ma, J. Z., Ma, Q. X., Zhang, P., Liu, Y. C., and He, H.: Effects of NO_2 and C_3H_6 on the heterogeneous oxidation of SO_2 on TiO_2 in the presence or absence of UV-Vis irradiation, Atmos. Chem. Phys., 19, 14777-14790, https://doi.org/10.5194/acp-19-14777-2019, 2019.

Davis, D. D., Ravishankara, A. R., and Fischer, S.: SO_2 oxidation via the hydroxyl radical: Atmospheric fate of HSO_x radicals, Geo. Res. Lett., 6, 113-116, https://doi.org/10.1029/GL006i002p00113, 1979.

Dentener, F., Carmichael, G., Zhang, Y., Lelieveld, J., and Crutzen, P.: Role of mineral aerosol as a reactive surface in the global troposphere, J. Geophy. Res.: Atmos., 101, 22869-22889, https://doi.org/10.1029/96jd01818, 1996.

Gen, M., Zhang, R., Huang, D., Li, Y., and Chan, C.: Heterogeneous oxidation of SO_2 in sulfate production during nitrate photolysis at 300 nm: Effect of pH, relative humidity, irradiation intensity, and the presence of organic compounds, Environ. Sci. Technol., 53, 8757-8766, https://doi.org/10.1021/acs.est.9b01623, 2019a.

Gen, M., Zhang, R., Huang, D., Li, Y., and Chan, C.: Heterogeneous SO_2 oxidation in sulfate formation by photolysis of particulate nitrate, Environ. Sci. Tech. Lett., 6, 86-91, https://doi.org/10.1021/acs.estlett.8b00681, 2019b.

Golobokova, L., Khodzher, T., Khuriganova, O., Marinayte, I., Onishchuk, N., Rusanova, P., and Potemkin, V.: Variability of chemical properties of the atmospheric aerosol above lake baikal during large wildfires in siberia, Atmosphere, 11, 1230-1250,

https://doi.org/10.3390/atmos11111230, 2020.

Gong, C., Yuan, X., Xing, D., Zhang, D., Martins-Costa, M. T. C., Anglada, J. M., Ruiz-Lopez, M. F., Francisco, J. S., and Zhang, X.: Fast sulfate formation initiated by the spin-forbidden excitation of SO_2 at the air-water interface, J. Am. Chem. Soc., 144, 22302-22308, https://doi.org/10.1021/jacs.2c10830, 2022.

Goodman, A., Li, P., Usher, C., and Grassian, V.: Heterogeneous uptake of sulfur dioxide on aluminum and magnesium oxide particles, J. Phys. Chem. A 105, 6109-6120, https://doi.org/10.1021/jp004423z, 2001.

Guo, S., Hu, M., Zamora, M. L., Peng, J., Shang, D., Zheng, J., Du, Z., Wu, Z., Shao, M., Zeng, L., Molina, M. J., and Zhang, R.: Elucidating severe urban haze formation in China, Proc. Natl. Acad. Sci. U. S. A., 111, 17373-17378, https://doi.org/10.1073/pnas.1419604111, 2014.

Harris, E., Sinha, B., van Pinxteren, D., Tilgner, A., Fomba, K. W., Schneider, J., Roth, A., Gnauk, T., Fahlbusch, B., Mertes, S., Lee, T., Collett, J., Foley, S., Borrmann, S., Hoppe, P., and Herrmann, H.: Enhanced role of transition metal ion catalysis during in-cloud oxidation of SO_2, Science, 340, 727-730, https://doi.org/10.1126/science.1230911, 2013.

He, G., Ma, J., and He, H.: Role of carbonaceous aerosols in catalyzing sulfate formation, ACS Catal., 8, 3825-3832, https://doi.org/10.1021/acscatal.7b04195, 2018a.

He, H., Li, C., Loughner, C. P., Li, Z., Krotkov, N. A., Yang, K., Wang, L., Zheng, Y., Bao, X., Zhao, G., and Dickerson, R. R.: SO_2 over central China: Measurements, numerical simulations and the tropospheric sulfur budget, J. Geophy. Res.: Atmos., 117, 37-51, https://doi.org/10.1029/2011jd016473, 2012.

He, P., Alexander, B., Geng, L., Chi, X., Fan, S., Zhan, H., Kang, H., Zheng, G., Cheng, Y., Su, H., Liu, C., and Xie, Z.: Isotopic constraints on heterogeneous sulfate production in Beijing haze, Atmos. Chem. Phys., 18, 5515-5528, https://doi.org/10.5194/acp-18-5515-2018, 2018b.

Herrmann, H., Ervens, B., Jacobi, H. W., Wolke, R., Nowacki, P., and Zellner, R.: CAPRAM$_{2.3}$: A chemical aqueous phase radical mechanism for tropospheric chemistry, J. Atmos. Chem., 36, 231-284, https://doi.org/10.1023/A:1006318622743, 2000.

Huang, L., Zhao, Y., Li, H., and Chen, Z.: Kinetics of heterogeneous reaction of sulfur dioxide on authentic mineral dust: Effects of relative humidity and hydrogen peroxide, Environ. Sci. Technol., 49, 10797-10805, https://doi.org/10.1021/acs.est.5b03930, 2015.

Hu, Q., Suzuki, H., Gao, H., Araki, H., Yang, W., and Noda, T.: High-frequency FTIR absorption of SiO_2/Si nanowires, Chem. Phys. Lett., 378, 299-304, https://doi.org/10.1016/j.cplett.2003.07.015, 2003.

Knopf, D., Cosman, L., Mousavi, P., Mokamati, S., and Bertram, A.: A novel flow reactor for studying reactions on liquid surfaces coated by organic monolayers: Methods, validation, and initial results, J. Phys. Chem. A, 111, 11021-11032, https://doi.org/10.1021/jp075724c, 2007.

Kroll, J., Frandsen, B., Kjaergaard, H., and Vaida, V.: Atmospheric hydroxyl radical source: Reaction of triplet SO_2 and water, J. Phys. Chem. A, 122, 4465-4469, https://doi.org/10.1021/acs.jpca.8b03524, 2018.

551 Langhammer, D., Kullgren, J., and Osterlund, L.: Photoinduced adsorption and oxidation of
552   SO_2 on anatase TiO_2, J. Am. Chem. Soc., 142, 21767-21774, https://doi.org/10.1021/jacs.0
553   c09683, 2020.
554 Li, G., Bei, N., Cao, J., Huang, R., Wu, J., Feng, T., Wang, Y., Liu, S., Zhang, Q., Tie, X., and
555   Molina, L. T.: A possible pathway for rapid growth of sulfate during haze days in China,
556   Atmos. Chem. Phys., 17, 3301-3316, https://doi.org/10.5194/acp-17-3301-2017, 2017.
557 Li, J., Zhang, Y. L., Cao, F., Zhang, W., Fan, M., Lee, X., and Michalski, G.: Stable sulfur
558   isotopes revealed a major role of transition-metal ion-catalyzed SO_2 oxidation in haze
559   episodes, Environ. Sci. Technol., 54, 2626-2634, https://doi.org/10.1021/acs.est.9b07150,
560   2020.
561 Li, K., Kong, L., Zhanzakova, A., Tong, S., Shen, J., Wang, T., Chen, L., Li, Q., Fu, H., and
562   Zhang, L.: Heterogeneous conversion of SO_2 on nano α-Fe_2O_3: the effects of morphology,
563   light illumination and relative humidity, Environ. Sci.: Nano, 6, 1838-1851,
564   https://doi.org/10.1039/c9en00097f, 2019.
565 Lim, S., Lee, M., Kim, S., and Laj, P.: Sulfate alters aerosol absorption properties in East Asian
566   outflow, Sci. Rep., 8, 5172-5178, https://doi.org/10.1038/s41598-018-23021-1, 2018.
567 Liu, T., Clegg, S., and Abbatt, J. P. D.: Fast oxidation of sulfur dioxide by hydrogen peroxide
568   in deliquesced aerosol particles, Proc. Natl. Acad. Sci. U. S. A., 117, 1354-1359,
569   https://doi.org/10.1073/pnas.1916401117, 2020a.
570 Liu, T., Chan, A. W. H., and Abbatt, J. P. D.: Multiphase oxidation of sulfur dioxide in aerosol
571   particles: Implications for sulfate formation in polluted environments, Environ. Sci.
572   Technol., 55, 4227-4242, https://doi.org/10.1021/acs.est.0c06496, 2021.
573 Liu, Y., Deng, Y., Liu, J., Fang, X., Wang, T., Li, K., Gong, K., Bacha, A. U., Nabi, I., Ge, Q.,
574   Zhang, X., George, C., and Zhang, L.: A novel pathway of atmospheric sulfate formation
575   through carbonate radicals, Atmos. Chem. Phys., 22, 9175-9197,
576   https://doi.org/10.5194/acp-22-9175-2022, 2022.
577 Ma, J., Dörner, S., Donner, S., Jin, J. L., Cheng, S. Y., Guo, J. R., Zhang, Z. F., Wang, J. Q.,
578   Liu, P., Zhang, G. Q., Pukite, J., Lampel, J., and Wagner, T.: MAX-DOAS measurements of
579   NO_2, SO_2, HCHO, and BrO at the Mt. Waliguan WMO GAW global baseline station in the
580   Tibetan Plateau, Atmos. Chem. Phys., 20, 6973-6990, https://doi.org/10.5194/acp-20-6973-
581   2020, 2020.
582 Ma, Q., Wang, L., Chu, B., Ma, J., and He, H.: Contrary role of H_2O and O_2 in the kinetics of
583   heterogeneous photochemical reactions of SO_2 on TiO_2, J. Phys. Chem. A., 123, 1311-1318,
584   https://doi.org/10.1021/acs.jpca.8b11433, 2019.
585 Martins-Costa, M., Anglada, J., Francisco, J., and Ruiz-Lopez, M.: Photochemistry of SO_2 at
586   the air-water interface: A source of OH and HOSO radicals, J. Am. Chem. Soc., 140, 12341-
587   12344, https://doi.org/10.1021/jacs.8b07845, 2018.
588 Mauldin, R., Berndt, T., Sipila, M., Paasonen, P., Petaja, T., Kim, S., Kurten, T., Stratmann, F.,
589   Kerminen, V., and Kulmala, M.: A new atmospherically relevant oxidant of sulphur dioxide,
590   Nature, 488, 193-196, https://doi.org/10.1038/nature11278, 2012.
591 Mukuta, T., Fukazawa, N., Murata, K., Inagaki, A., Akita, M., Tanaka, S., Koshihara, S. Y., and
592   Onda, K.: Infrared vibrational spectroscopy of $[Ru(bpy)_2(bpm)]^{2+}$ and $[Ru(bpy)_3]^{2+}$ in the

593   excited triplet state, Inorg. Chem., 53, 2481-2490, https://doi.org/10.1021/ic402474t, 2014.

594 Olson, E., Michalski, G., Welp, L., Valdivia, A., Larico, J., Pen, J., Fang, H., Gomez, K., and
595   Li, J.: Mineral dust and fossil fuel combustion dominate sources of aerosol sulfate in urban
596   Peru identified by sulfur stable isotopes and water-soluble ions, Atmos. Environ., 260,
597   118482-118495, https://doi.org/10.1016/j.atmosenv.2021.118482, 2021.

598 Park, J. and Jang, M.: Heterogeneous photooxidation of sulfur dioxide in the presence of airborne
599   mineral dust particles, RSC Adv., 6, 58617-58627, https://doi.org/10.1039/c6ra09601h,
600   2016.

601 Park, J., Jang, M., and Yu, Z.: Heterogeneous photo-oxidation of SO_2 in the presence of two
602   different mineral dust particles: Gobi and arizona dust, Environ. Sci. Technol., 51, 9605-
603   9613, https://doi.org/10.1021/acs.est.7b00588, 2017.

604 Peng, Y., von Salzen, K., and Li, J.: Simulation of mineral dust aerosol with Piecewise Log-
605   normal Approximation (PLA) in CanAM4-PAM, Atmos. Chem. Phys., 12, 6891-6914,
606   https://doi.org/10.5194/acp-12-6891-2012, 2012.

607 Prospero, J.: Long-range transport of mineral dust in the global atmosphere: Impact of African
608   dust on the environment of the southeastern United States, Proc. Natl. Acad. Sci. U. S. A.,
609   96, 3396-3403, https://doi.org/10.1073/pnas.96.7.3396, 1999.

610 Shao, J., Chen, Q., Wang, Y., Lu, X., He, P., Sun, Y., Shah, V., Martin, R. V., Philip, S., Song,
611   S., Zhao, Y., Xie, Z., Zhang, L., and Alexander, B.: Heterogeneous sulfate aerosol formation
612   mechanisms during wintertime Chinese haze events: air quality model assessment using
613   observations of sulfate oxygen isotopes in Beijing, Atmos. Chem. Phys., 19, 6107-6123,
614   https://doi.org/10.5194/acp-19-6107-2019, 2019.

615 Shiraiwa, M., Ueda, K., Pozzer, A., Lammel, G., Kampf, C. J., Fushimi, A., Enami, S., Arangio,
616   A. M., Frohlich-Nowoisky, J., Fujitani, Y., Furuyama, A., Lakey, P. S. J., Lelieveld, J., Lucas,
617   K., Morino, Y., Poschl, U., Takahama, S., Takami, A., Tong, H., Weber, B., Yoshino, A., and
618   Sato, K.: Aerosol health effects from molecular to global scales, Environ. Sci. Technol., 51,
619   13545-13567, https://doi.org/10.1021/acs.est.7b04417, 2017.

620 Sidebottom, H. W., Badcock, C. C., Jackson, G. E., Calvert, J. G., Reinhardt, G. W., and Damon,
621   E. K.: Photooxidation of sulfur dioxide, Environ. Sci. Technol., 6, 72-79,
622   https://doi.org/10.1080/00022470.1971.10469552, 1972.

623 Solbrig, C. W. and Gidaspow, D.: Convective diffusion in a parallel plate duct with one catalytic
624   wall, laminar flow, first order reaction-part one, Can. J. Chem. Eng., 45, 35-39,
625   https://doi.org/10.1016/0304-5102(89)80197-X, 1967.

626 Sumner, A. L., Menke, E. J., Dubowski, Y., Newberg, J. T., Penner, R. M., Hemminger, J. C.,
627   Wingen, L. M., Brauers, T. and Finlayson-Pitts, B. J. The nature of water on surfaces of
628   laboratory systems and implications for heterogeneous chemistry in the troposphere. Phys.
629   Chem. Chem. Phys., 6, 604-613, https://doi.org/10.1039/B308125G, 2004.

630 Tohidi, R., Farahani, V., and Sioutas, C.: Real-time measurements of mineral dust concentration
631   in coarse particulate matter $PM_{10-2.5}$ by employing a novel optical-based technique in Los
632   Angeles, Sci. Total. Environ., 838, 156215-156226, https://doi.org/10.1016/j.scitotenv.202
633   2.156215, 2022.

634 Urupina, D., Romanias, M. N., and Thevenet, F.: How relevant is it to use mineral proxies to

mimic the atmospheric reactivity of natural dust samples? A reactivity study using SO_2 as probe molecule, Minerals, 11, 282-299, https://doi.org/10.3390/min11030282, 2021.

Urupina, D., Lasne, J., Romanias, M. N., Thiery, V., Dagsson-Waldhauserova, P., and Thevenet, F.: Uptake and surface chemistry of SO_2 on natural volcanic dusts, Atmos. Environ., 217, 116942-116959, https://doi.org/10.1016/j.atmosenv.2019.116942, 2019.

Usher, C., Michel, A., and Grassian, V.: Reactions on mineral dust, Chem. Rev. , 103, 4883-4939, https://doi.org/10.1021/cr020657y, 2003.

Usher, C., Al-Hosney, H., Carlos-Cuellar, S., and Grassian, V.: A laboratory study of the heterogeneous uptake and oxidation of sulfur dioxide on mineral dust particles, J. Geophys. Res-atmos. , 107, 4713-4729, https://doi.org/10.1029/2002jd002051, 2002.

Wang, J., Li, J., Ye, J., Zhao, J., Wu, Y., Hu, J., Liu, D., Nie, D., Shen, F., Huang, X., Huang, D. D., Ji, D., Sun, X., Xu, W., Guo, J., Song, S., Qin, Y., Liu, P., Turner, J. R., Lee, H. C., Hwang, S., Liao, H., Martin, S. T., Zhang, Q., Chen, M., Sun, Y., Ge, X., and Jacob, D. J.: Fast sulfate formation from oxidation of SO_2 by NO_2 and HONO observed in Beijing haze, Nat. Commun., 11, 2844-2850, https://doi.org/10.1038/s41467-020-16683-x, 2020a.

Xu, M., Qiu, P., He, Y., Guo, S., Bai, Y., Zhang, H., Zhao, S., Shen X., Zhu, B., Guo, Q., Guo, Z., Sulfur isotope composition during heterogeneous oxidation of SO_2 on mineral dust: The effect of temperature, relative humidity, and light intensity. Atmos. Res., 254, 105513, https://doi.org/10.1016/j.atmosres.2021.105513, 2021.

Yao, M., Zhao, Y., Hu, M., Huang, D., Wang, Y., Yu, J. Z., and Yan, N.: Multiphase reactions between secondary organic aerosol and sulfur dioxide: Kinetics and contributions to sulfate formation and aerosol aging. Environ. Sci. Technol. Lett., 6, 768-774, https://doi.org/10.1021/acs.estlett.9b00657, 2019.

Ye, J., Abbatt, J. P. D., Chan, A. W. H.: Novel pathway of SO_2 oxidation in the atmosphere: Reactions with monoterpene ozonolysis intermediates and secondary organic aerosol. Atmos. Chem. Phys., 18, 5549-5565, https://doi.org/10.5194/acp-18-5549-2018, 2018.

Wang, S., Zhou, S., Tao, Y., Tsui, W. G., Ye, J., Yu, J. Z., Murphy, J. G., McNeill, V. F., Abbatt, J. P. D., and Chan, A. W. H.: Organic peroxides and sulfur dioxide in aerosol: Source of particulate sulfate. Environ. Sci. Technol., 53, 10695-10704, https://doi.org/10.1021/acs.est.9b02591, 2019.

Wang, T., Liu, Y., Deng, Y., Fu, H., Zhang, L., and Chen, J.: The influence of temperature on the heterogeneous uptake of SO_2 on hematite particles, Sci. Total. Environ., 644, 1493-1502, https://doi.org/10.1016/j.scitotenv.2018.07.046, 2018.

Wang, T., Liu, Y. Y., Deng, Y., Cheng, H. Y., Yang, Y., Li, K. J., Fang, X. Z., and Zhang, L. W.: Irradiation intensity dependent heterogeneous formation of sulfate and dissolution of ZnO nanoparticles, Environ. Sci.: Nano, 7, 327-338, https://doi.org/10.1039/c9en01148j, 2020b.

Wang, Z., Wang, T., Fu, H., Zhang, L., Tang, M., George, C., Grassian, V. H., and Chen, J.: Enhanced heterogeneous uptake of sulfur dioxide on mineral particles through modification of iron speciation during simulated cloud processing, Atmos. Chem. Phys., 19, 12569-12585, https://doi.org/10.5194/acp-19-12569-2019, 2019.

Yang, N., Tsona, N. T., Cheng, S., Li, S., Xu, L., Wang, Y., Wu, L., and Du, L.: Competitive reactions of SO_2 and acetic acid on α-Al_2O_3 and $CaCO_3$ particles, Sci. Total. Environ., 699,

134362-134370, https://doi.org/10.1016/j.scitotenv.2019.134362, 2020.

Yang, W., Ma, Q., Liu, Y., Ma, J., Chu, B., and He, H.: The effect of water on the heterogeneous reactions of SO_2 and NH_3 on the surfaces of α-Fe_2O_3 and γ-Al_2O_3, Environ. Sci.: Nano, 6, 2749-2758, https://doi.org/10.1039/c9en00574a, 2019.

Zhang, P., Chen, T., Ma, Q., Chu, B., Wang, Y., Mu, Y., Yu, Y., and He, H.: Diesel soot photooxidation enhances the heterogeneous formation of H_2SO_4, Nat. Commun., 13, 5364-5372, https://doi.org/10.1038/s41467-022-33120-3, 2022.

Zhang, R., Gen, M., Huang, D., Li, Y., and Chan, C.: Enhanced sulfate production by nitrate photolysis in the presence of halide ions in atmospheric particles, Environ. Sci. Technol., 54, 3831-3839, https://doi.org/10.1021/acs.est.9b06445, 2020a.

Zhang, T., Yang, W., Han, C., Yang, H., and Xue, X.: Heterogeneous reaction of ozone with syringic acid: Uptake of O_3 and changes in the composition and optical property of syringic acid, Environ. Pollut., 257, 113632-113638, https://doi.org/10.1016/j.envpol.2019.113632, 2020b.

Zhang, X., Zhuang, G., Chen, J., Wang, Y., Wang, X., An, Z., and Zhang, P.: Heterogeneous reactions of sulfur dioxide on typical mineral particles, J. Phys. Chem. B, 110, 12588-12596, https://doi.org/10.1021/jp0617773, 2006.

Zhang, Y., Bao, F., Li, M., Chen, C., and Zhao, J.: Nitrate-enhanced oxidation of SO_2 on mineral dust: A vital role of a proton, Environ. Sci. Technol., 53, 10139-10145, https://doi.org/10.1021/acs.est.9b01921, 2019.

Zhang, Y., Bao, F., Li, M., Xia, H., Huang, D., Chen, C., and Zhao, J.: Photoinduced uptake and oxidation of SO_2 on Beijing urban $PM_{2.5}$, Environ. Sci. Technol., 54, 14868-14876, https://doi.org/10.1021/acs.est.0c01532, 2020c.